ELSEVIER

Journal of Power Sources 102 (2001) 270–276

JOURNAL OF POWER SOURCES

www.elsevier.com/locate/jpowsour

The ac impedance studies for porous MnO_2 cathode by means of modified transmission line model

Deyang Qu*

Rayovac Corporation, 601 Rayovac Dr., Madison, WI 53711, USA

Received 2 April 2001; received in revised form 27 April 2001; accepted 1 May 2001

Abstract

A simplified 5-RC transmission line equivalent circuit was introduced. Manganese dioxide cathodes from three commercial primary alkaline cells were investigated by means of ac impedance technique. Cathode Ohmic resistance, Faraday resistance for the reduction of MnO_2, proton diffusion rate inside the lattice of EMD and electrochemical accessible surface area were obtained by numerical fitting of impedance data using the simplified transmission line model. The kinetics for cathode surface accessibility was also studied.

Keywords: Manganese dioxide cathode; Alkaline battery; Impedance; Transmission line model; Porous electrode

1. Introduction

The growth of modern electronic devices such as the digital camera, cell phone and high-tech toys, requires the battery to be better suited for high power application. Despite significant advancements in the development and commercialization of new battery systems, alkaline MnO_2–Zn cells still dominate the consumer battery market. Thus, developing alkaline MnO_2/Zn cells, which can be discharged at high rate, becomes the challenge for all battery manufactures.

2. Formation of the problems

2.1. Electrolyte transportation within the cathode matrix

A porous electrode, such as the MnO_2 cathode, consists of an electronically conductive solid medium with a high surface area and electrolyte-filled pores. The three-dimensional electrode gives high surface area to volume ratios with a high availability of reacting electrolyte-electrode interfacial area as a result. Such an electrode configuration finds particular application in cases of relatively slow electrode reactions, insoluble reactants or products, and non-conducting active materials. The kinetics of mass transfer is directly related to the porous structure of the electrode.

In an alkaline system, the MnO_2 cathode is described as one of the limitations for high rate discharge.

Mass transfer phenomena play a dominating role in the function of an EMD cathode. A close investigation requires a separation of effects contributed by different transport processes. Two of those processes involve electrolyte diffusion inside the matrix of the porous electrode, through pores of various sizes and proton diffusion throughout the lattice of MnO_2. The first process relates to the pores formed by the manganese dioxide particles in conjunction with the graphite and other non-active ingredients. The other one relates to EMD properties such as crystal structure, grain boundary, etc.

Most electrochemical investigations of manganese dioxide electrodes ignored the porosity of the electrode, assuming that the influence can be eliminated by use of low EMD to graphite ratio, flooded electrolyte and thin electrode [1–3]. Even though valuable conclusions regarding the reduction mechanism of EMD [4–6] were drawn from the results obtained this way, ignoring the impact of cathode porosity is not valid for commercial EMD cathodes in primary and secondary alkaline MnO_2– Zn cells, since all the cathodes in those cells are in bobbin design with a high EMD to graphite ratio and are starved for electrolyte in order to ensure high energy density.

The electrode fabrication processes also determine the porous structure for an EMD cathode. Each EMD electrode,

* Tel.: +1-608-275-4745.
E-mail address: qu@rayovac.com (D. Qu).

0378-7753/01/$ – see front matter
PII: S0378-7753(01)00810-2

manufactured by means of different industrial processes, has its unique pore distribution. Pores with different sizes have different time constants. This means that, not all the pores can be accessed electrochemically and certainly not in the same time scale. Electrochemically accessible surface area is normally smaller than the BET surface area. Designing an electrode that allows more internal surface area to be accessed more quickly is the key to achieving high rate capability for an alkaline manganese dioxide cathode.

The surface area of a given mass of solid material is inversely related to the size of the constituent particles. In practice, the particles of a fine powder, the primary particles [7], will stick together because of the surface forces to form secondary particles. Pores are formed in those aggregated particles. Pore size depends on the size and shape of primary particles and how they are packed together. So the surface area of a solid can be conveniently distinguished between the external and internal surface. The external surface includes all the outer surface of secondary particles, and all of those cracks that are wider than they are deep. The internal surface will then comprise the walls of all cracks, pores and cavities that are deeper than they are wide. Obviously, external surface is much easier to be accessed by electrolyte than internal surface.

In-depth studies have been conducted by Soffer Folman [8], Koresh and Sofer [9], and more recently by Qu and Shi [10], regarding the accessibility of micropores to aqueous solutions. It has been concluded that since the size of a single N_2 molecule is similar to that of OH^- or K^+ ions in aqueous solution, those micropores that can accommodate adsorbed nitrogen molecules at 77 K are also available for electro-adsorption of simple hydrated ions at low, concentration-dependent rate. In principal, pores whose sizes are larger then 5 Å could be eventually accessible electrochemically. Of course, the surface area of pores with different pore width has different time constants. In other words, the electrolyte diffusion rate inside pores of various sizes is different. Qu and Shi [10] established the relationship between the accessible time constant and the pore diameter for activated carbon electrode using a transmission line model. In this paper, a simplified transmission line model is introduced in which the Faraday reaction of manganese dioxide and the Warberg impedance for proton diffusion inside the crystal lattice of EMD were taken into consideration.

2.2. Proton insertion

Proton insertion into the solid phase of EMD has been extensively studied and a heterogeneous ''proton-hopping'' reaction mechanism for the first electron insertion has been well adopted. The reduction can be written as

$$MnO_2 + H_2O + e^- \rightarrow MnOOH + OH^-$$

The electrochemical reaction happens at the EMD/electrolyte interface, then the protons diffuse into the bulk of the particles. In general, reduction of manganese dioxide contains three consequent steps:

- H_2O decomposition at the surface of manganese dioxide particles;
- proton intercalation into the crystal structure;
- proton diffusion into the bulk of particles.

Charge transfer, adsorption at the surface, and mobility of protons are critical processes during the reduction. The surface condition of EMD particles, including surface functional groups and crystal orientation on the surface, may play an important role for H_2O decomposition, while the crystal structure of EMD definitely determines the charge transfer and proton diffusion processes. These structural parameters may include De Wolf disorder [11], microtwinning [12], cation vacancy [13,14], crystal size/grain boundary and stress for a particular EMD material.

3. Experimental

Samples of LR6 (AA) primary alkaline MnO_2/Zn batteries were purchased from the open market. Samples, purchased at the same, of a particular type of cell were used to conduct the experiments in order to avoid possible formulation changes. Sealed Zn reference electrodes were implanted into the cathode/separator interface of test cells according to the procedures reported by Barnard et al. [15]. The impedance of the cathode included can-cathode contact and the cathode itself, but excluded the separator and anode.

All experiments were done at room temperature (298 ± 1 K).

The ac impedance measurements were conducted by means of Solaritron Electrochemical Interface 1255 and Solaritron Frequency Response Analyzer controlled by ZPLOT. All equivalent circuit fittings for impedance results were done by either ZVIEW or home made software.

All the cells were discharged under 330 mA constant current. The discharge of the each cell was stopped at 0 min (fresh cell), 20, 50, 150 and 200 min. Cells were put on rest until the potential variation between the cathode and the implanted Zn reference electrode became less than ± 5 mV. The ac impedance measurements were then carried out at OCV and ± 10 mV potential amplitude.

4. Results and discussion

The ac impedance technique has been extensively used to investigate intercalation cathodes by means of numerical fitting with various equivalent circuits. A lot of excellent works were reported, for example, γ-MnO_2 in KCl solution by Atlung and Jacobsen [16], TiS_2 by Narayanan et al. [17] and $Li_{1-x}CoO_2$ by Thomas et al. [18]. However, most of these previous works were done under a well-controlled environment in lab cells with simplified electrode formulation.

The results reported in this paper are from "real-life" commercial cathodes.

4.1. Mechanism and equivalent circuits

Fig. 1 shows the general transmission line model [19]. Distributed capacitance and resistance are used to represent energy dissipation in a porous electrode, while Faraday resistance and Warberg impedance are used to simulate charge transfer and proton diffusion inside manganese dioxide particles, respectively.

A porous electrode that involves Faraday charge transfer, can be thought of as a "leaked" capacitor. Two types of current inside the electrode matrix should be distinguished. They are, the current due to proton insertion and electron migration inside EMD particles (leakage current, I_f) and non-Faraday current to charge/discharge double layer. In our system the Faraday current was much higher.

R_{ct} in Fig. 1 is the charge transfer resistance and can be represented as

$$R_{ct} = \frac{RT}{mFi_0} \tag{1}$$

where i_0 is exchange current, which can be represented as

$$i_0 = \frac{1}{V_m}\left\{nFAk^0 C_{H^+}^{1/2}[x(1-x)]^{1/2}\right\} \tag{2}$$

then

$$R_{ct} = \frac{RTV_m}{n^2F^2Ak^0C_{H^+}^{1/2}}[x(1-x)]^{-1/2} \tag{3}$$

C_{H^+} is the concentration of protons at the surface of the cathode; k^0 is the standard rate constant for the heterogeneous reaction, V_m is the mole volume of the solid, x is the mole fraction of MnO_2.

In Fig. 1, Z_w represents the Warburg impedance. In the case of semi-infinite diffusion ($\omega \gg D/l^2$), it can be written as

$$Z_w = \sigma(1-i)\omega^{-1/2} \tag{4}$$

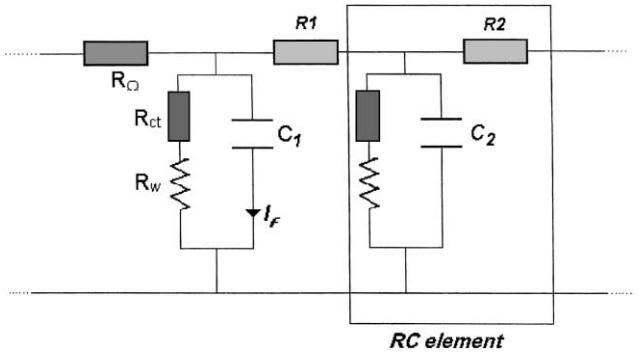

Fig. 1. Transmission Line equivalent circuit. Simplified circuit consists 5-RC components.

where

$$\sigma = \frac{V_m}{nFA(2D)^{1/2}}\frac{\partial V_{oc}}{\partial x} \tag{5}$$

where D is the chemical diffusion coefficient; l diffusion length and $\partial V_{oc}/\partial x$ is the slope of the open-circuit voltage V_{oc} versus mole fraction of MnO_2.

In the case in which ac signal penetration depth is comparable to the depth of the pores, the situation can be analogous to a RC transmission line network. The mathematical equation of the transmission line has the same form as the diffusion equation since the process taking place in an RC circuit may be treated as electronic diffusion into a semi-infinite medium. Its impedance can be represented as

$$Z = \sigma'\omega^{-m}\left[\cos(\tfrac{1}{2}m\pi) - \mathrm{i}\sin(\tfrac{1}{2}m\pi)\right] \quad (0 < m < 1) \tag{6}$$

where σ' is termed as the constant phase element (CPE) factor; m the CPE exponent. When $m = 1/2$, Eq. (6) is identical to Eq. (4).

The number of RC elements in the general form of transmission line, as shown in Fig. 1, should be infinite. Each element stands for $1/n$ ($n \to \infty$) percent of electrode surface area. To simplify the calculation, during the studies for MnO_2 cathode, the equivalent circuit was simplified to 5-RC components. Each stood for 20% of the electrochemically accessible surface area.

Assuming the specific capacitance (F/cm^2) for MnO_2 cathode is the same, the double layer capacitance should be proportional to the electrochemical accessible surface area, $C_1 = C_2 = C_3 = C_4 = C_5 = C$. Since the cathode should be uniform, R_{ct} and Z_w of each RC elements should be the same. $R_1, R_2, \ldots, R_5$ can be regarded as the measurements of how difficult it is to electrochemically access the projected surface area or pores [10].

Fig. 2 shows the complex plane plot for Brand B cathode for both experimental data and the fitting results based on the simplified equivalent circuit. In Fig. 2, the same cathode was

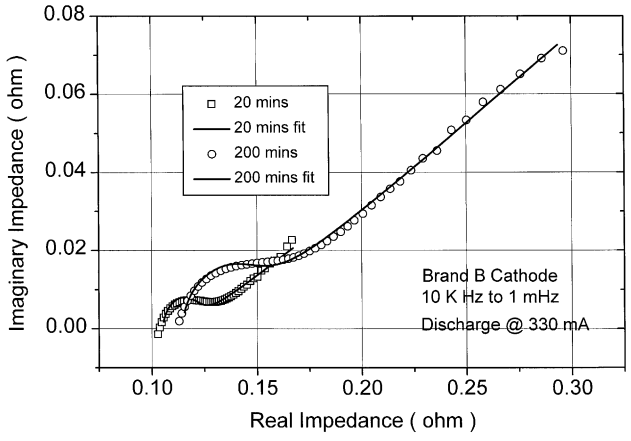

Fig. 2. Comparison of typical impedance complex planes for an MnO_2 cathode. The results represent cathode B discharge at 330 mA for 20 and 200 min.

Table 1
Fitting results based on equivalent circuit shown in Fig. 1

Parameters	Discharged (20 min)	Discharged (200 min)
Ohmic resistance (R_Ω)	0.10518	0.1145
Charge transfer resistance (R_{ct})	0.0329	0.0649
Double layer capacitance (C_{dl})	0.00436	0.00171
Warburg perfactor (σ)	0.221	0.787
R_1	0.000253	2.253e-5
R_2	0.021358	0.028576
R_3	0.02259	0.022391
R_4	0.049325	0.007724
R_5	0.48633	1.623

discharged at 330 mA for 20 and 200 min before the impedance measurements took place. Excellent fitting has been obtained. The results are given in Table 1.

4.2. Ohmic resistance R_Ω

R_Ω is the real component of the complex impedance at $\omega \rightarrow \infty$ for the equivalent circuit shown in Fig. 1. Since R_Ω is a parameter determined in the frequency limit, the value cannot be obtained unless a complete interpretation of the complex plane impedance behavior is available. The Ohmic resistance of a primary alkaline manganese dioxide cathode contains:

1. electrolyte resistance;
2. contact resistance between can and consolidated cathode;
3. contact resistance among the particles that constitute the electrode materials;
4. intrinsic resistance of electrode materials themselves.

Separation of R_Ω into its constituent components is not possible using the current equivalent circuit in the present analysis. Multiple reference electrode implantation and chemical analysis are needed for the separation.

Fig. 3 shows the comparison of Ohmic resistance change for the three cathodes during 330 mA discharge. Cathode A demonstrated the best conductivity throughout the course of discharge. The conductivities for cathode B were very close to those of cathode A, while the conductivities of cathode C were much lower. The difference resulted from the relative contribution from various components to the total resistance. The relative contribution clearly varies considerably with cell assembly, electrolyte concentration, density, cathode design, cathode geometry, and quality of electrode material.

4.3. Double layer capacitance and electrochemical accessible surface area

Helmoholtz in 1879 [20], Gouy in 1910 [21], Chapman in 1913 [22] and Stern in 1924 [23] discovered that charges can be separated and form a double layer across a conductor and liquid electrolyte. The capacitance stored in the double layer

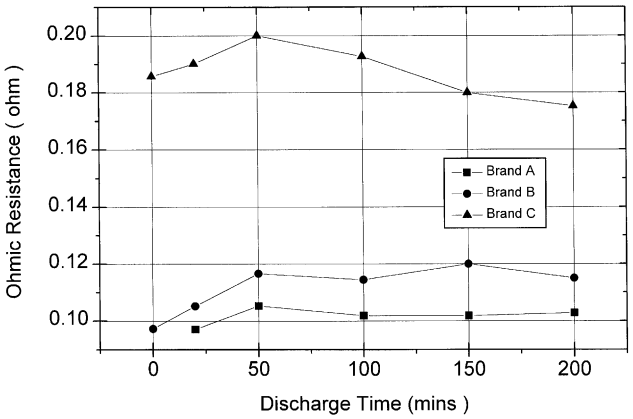

Fig. 3. Comparison of Ohmic resistance, R_Ω changes for the three cathodes at various stages of 330 mA discharge.

is proportional to the surface area of the electrode and inversely proportional to the thickness of the double layer. Since strong KOH solution is used in all alkaline MnO_2 cathodes, and the ratio between EMD and graphite is similar (Not the same!), the double layer capacitance of a cathode can be treated as proportional to the surface area with the establishment of a double layer. This surface area is electrochemically accessible.

It is always desirable to have a high accessible surface area for MnO_2 cathode. Fig. 4 shows the comparison of the double layer capacitance for the three cathodes at various stages of discharge. It can be observed that although the double layer capacitance became similar for all three electrodes in the later stage of discharge, cathode A had much higher double layer capacitance initially. In other words, initial electrochemically accessible surface area for cathode A was much higher than those of the other two. It also worth noticing that cathode B only improved marginally as compared to cathode C. The different accessible surface area primarily results from cathode fabrication processes and choice of cathode ingredients. The decrease of the

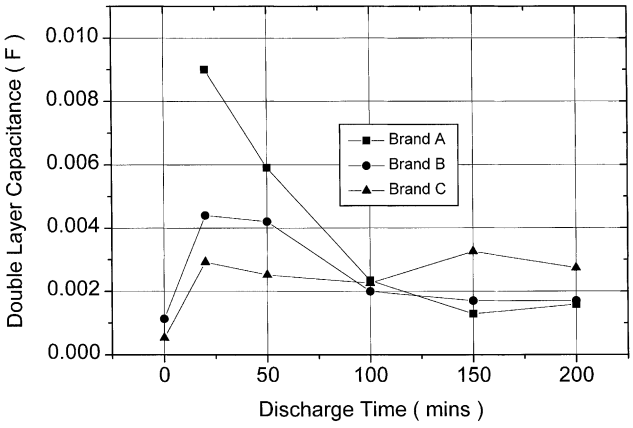

Fig. 4. Comparison of double layer capacitance (C) charges for the three cathodes at various stages of 330 mA discharge. Double layer capacitance is proportional to electrochemically accessible surface area.

surface area during discharge was believed to result from the expansion of the MnO_2 particles. As the volume of the cathode changed, some pores, especially those with small openings, could be sealed, thus reducing the surface area.

4.4. Charge transfer resistance R_{ct}

The single EMD electrode potential varies with the extent of proton intercalation. It can be assumed to be invariant with the state of charge of the cell. Thus, the studies at various values of open circuit cell voltage could reflect changes in the equilibrium properties of the cathode.

Fig. 5 shows the comparison of R_{ct} for the three cathodes at various stages during 330 mA discharge. As shown in Eq. (3), R_{ct} is proportional to $1/k^0$, k^0 is the standard rate constant for the heterogeneous reaction. R_{ct} is believed to relate to the surface condition of EMD particles. Comparing R_{ct}'s for the three cathodes, one can observe that EMD in cathode A was very similar to that in B cathode. Both should outperform the EMD in cathode C, since R_{ct}'s for the EMD in both cathode A and cathode C were much lower than that of cathode B, except for the initial stage of discharge. R_{ct} is determined by the quality of EMD and has little relationship with cathode structure. High R_{ct} will result of high electrochemical overpotential during discharge.

4.5. Warburg prefactor σ

The values of the Warburg prefactor, σ corresponding to the element ω, can be evaluated from non-linear least square analysis based on Eq. (4). In our case, the Warburg impedance, as shown in Fig. 1, described the proton diffusion step in the EMD lattice. As shown in Eq. (5), Warburg prefactor is proportional to $1/\sqrt{D}$, where D is the proton diffusion coefficient. Theoretically, the actual proton diffusion coefficient can be extracted from Eq. (5), since both V_m and $\partial V_{oc}/\partial x$ are experimentally obtainable parameters. Practically, $\partial V_{oc}/\partial x$ can be measured from discharge curve of ultra low current density. It is rather tricky to measure V_m, since EMD crystal cells expand during discharge. The degree of expansion is related to the characteristics of EMD. In very well controlled experimental conditions, we have successfully calculated proton diffusion coefficient for a known EMD through Eq. (5). V_m changes due to the expansion during the discharge were taken into consideration and the results will be reported elsewhere. In the current case, however, the cathode samples were from primary alkaline cells purchased from the open market. The characteristics of the EMD are unknown and measuring the cathode volume change is difficult. We did not attempt to measure exact proton diffusion coefficient for the three cathodes. However, Warburg prefector can still be used as an indicator for proton diffusion rate.

Fig. 6 shows the comparison of Warburg prefactor σ for the three cathodes during 330 mA discharge. It is obvious that proton diffusion rates for cathode A and cathode B were similar and higher than that of cathode C. We may conclude that the EMD used in cathode A and cathode B had similar quality and were better than that of cathode C. The conclusion is consistent with that in 4.4.

4.6. Kinetics for electrode surface accessibility

The situation in a porous electrode differs in important ways from that of a simple series RC circuit. The essential difference between a porous electrode and a planar one lies in the distribution of the double layer capacitance coupled in series-parallel ways with the solution resistance. In this case, small but significantly with the resistance of the matrix of the porous material. Thus, for a porous electrode the IR-drop, Ohmic dissipation of energy, I^2R, and ion transfer rate are no longer single-valued quantities at a given current, but vary down the pore. The local I, which is determined by local ion and electron transfer rate, diminishes and the cumulative resistance increases owing to a continuous increase of electrolytic resistance down the pore from its orifice.

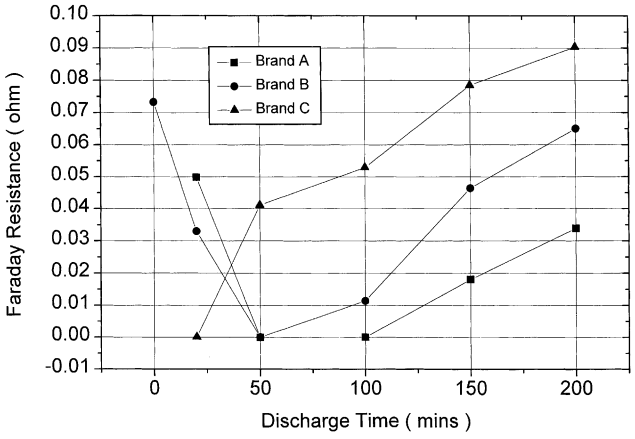

Fig. 5. Comparison of Faraday resistance (R_{ct}) changes for the three cathodes at various stages of 330 mA discharge.

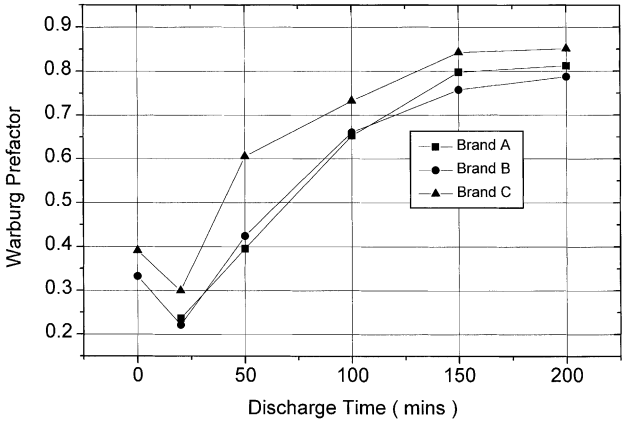

Fig. 6. Comparison of Warburg prefactor (σ) changes at various stages of 330 mA discharge for the three cathodes. Warbug perfactor is proportional to $1/\sqrt{D}$, D is proton diffusion coefficient.

Consequently, any discharge signal does not have an immediate and uniform effect on the time-dependent state of discharge of the electrode. No unique time constant characterizes the response function for such an electrode subject to ac modulation and the impedance is substantially frequency dependent. The "penetration depth" for a pore depends on the conductivity, the diameter of the pore opening, and the frequency of modulation (alternatively, discharge current density). At high frequencies, only the *C–R* of larger pore and the outer orifice region of the small pores are modulated so the measured capacitance/resistance becomes dispersed to that of only the projected surface area of the porous electrode. Thus, the surface area of pores with different openings can only be accessed at certain ac frequency. Integrated energy dissipation should be calculated in order to evaluate efficiency of discharging as a function of rate. The "penetration depth" or surface utilization at a certain frequency is mass transfer and electron transfer rate related; it relies not only on the porosity, but also the conductivity of the electrode matrix.

In the simplified 5-RC circuit, each RC projects 20% of electrochemically accessible surface area. *R* is proportional

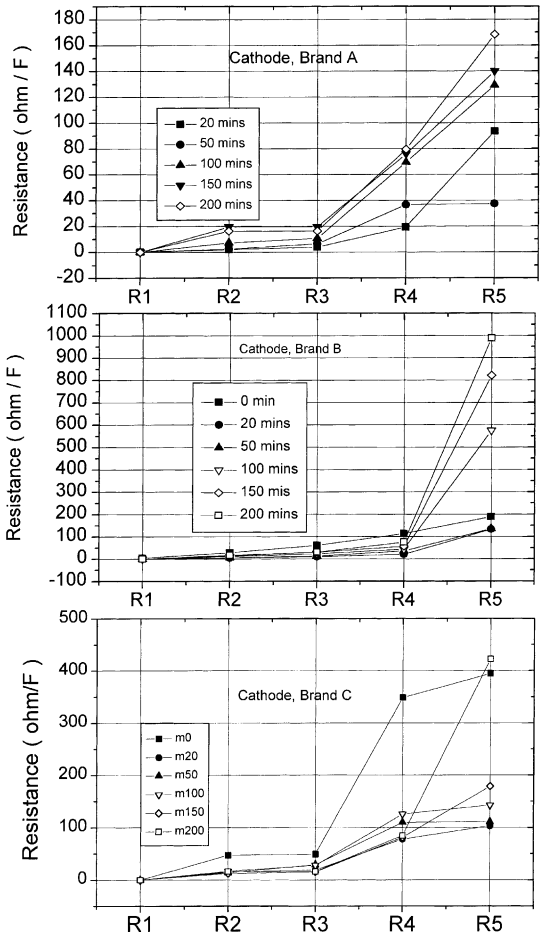

Fig. 7. Comparison of accumulated distributed resistance changes at various stages of 330 mA discharge. The results for cathodes from brands A, B, C are shown in the separate graph.

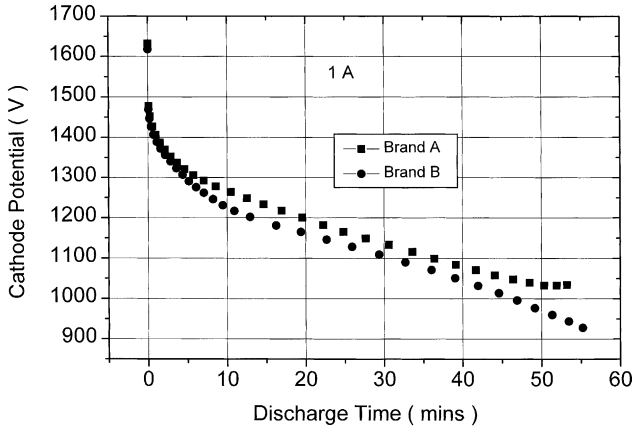

Fig. 8. Comparison of 1A discharge curves for cathodes from brands A and B.

to the difficulty of accessing the projected portion of cathode surface. The "penetration depth" is from R_1C to R_5C. R_1C represents the most accessible 20% of the cathode surface area, which mainly consists of the outer surface area and the surface area of large pores. R_5C represents the most difficult 20% of the surface area to access, which mainly consists of pores with small openings.

Fig. 7 show the comparison of accumulated *R* for the three cathodes. The calculated resistance was defined as *R*/*C* (Ω/F), which describes resistance per unit surface area. The first 60% of the cathode surface area is easy to utilize for all three cathodes. The accessibility for the last 40% differed from cathode to cathode. From Fig. 7, two things are worth pointing out. First, all (100%) of cathode A's electrode surface area was easy to access, while the surface area of cathode C seems more accessible than that of cathode B, especially for the last 20% of electrode surface. Second, the mass transfer becomes more difficult as discharge continues. The most severe changes were observed for the last 20% of electrode surface. The phenomenon is believed to result from cathode expansion during discharge. The pores with fine openings are easily sealed during cathode volume change, thus mass transfer in and out of these pores becomes more difficult. The observation is consistent with what is described in 4.3.

4.7. Cathode discharge curve

Fig. 8 shows the comparison of the cathode discharge curve for cell A and cell B. The cathodes were discharged at 1 A against an implanted Zn reference electrode.

5. Conclusions:

The nature of the MnO_2 primary alkaline cathode that is responsible for its electrochemical performance, especially high rate has, been elucidated using impedance and a simplified equivalent circuit, which is derived from the traditional transmission line model. The validity of the

circuit was exemplified on cathodes of three commercial primary cells. The following points are of value to be noted.

1. The performance for a MnO_2 cathode depends on the quality of EMD, conductivity of the cathode, and most importantly, a porous cathode structure that favors fast mass transfer.
2. The quality of EMD can be measured in terms of the Faraday resistance (exchange current) and the proton diffusion rate inside the lattice of EMD.
3. Electrochemically accessible surface area can be represented by double layer capacitance.
4. Distributed resistances can roughly gauge mass transfer inside the matrix.
5. The superior performance for the cathode resulted from the use of a high grade EMD and a properly engineered cathode.

References

[1] N.C. Cahoon, J. Electrochem. Soc. 99 (1952) 343.
[2] A.B. Scott, J. Electrochem. Soc. 107 (1960) 941.
[3] A. Kozawa, R.A. Powers, J. Electrochem. Soc. 106 (1959) 745.
[4] G.S. Bell, R. Huber, J. Electrchem. Soc. 111 (1964) 1.
[5] A. Kozawa, J.F. Yeager, J. Electrochem. Soc. 115 (1968) 1003.
[6] J. McBreen, Power Source 5 (1975) 525.
[7] S.J. Gregg, K.S.W. Sing, Adsorption, Surface Area and Porosity, Academic Press, London, 1982.
[8] A. Soffer, N. Folman, J. Electroanal. Chem. 25 (1972) 38.
[9] J. Koresh, A. Soffer, J. Electroanal. Chem. 147 (1983) 223.
[10] D.Y. Qu, H. Shi, J. Power Source 74 (1998) 99.
[11] P.M. De Wolff, Acta Crystallogr. 12 (1959) 341.
[12] Y. Chabre, J. Pannetier, Prog. Solid St. Chem. 23 (1995) 1.
[13] P. Ruetsch, J. Electrchem. Soc. 135 (1988) 2657.
[14] P. Ruetsch, R Giovanoli, J. Elctrochem. Soc. 135 (1998) 2663.
[15] R. Barnard, L.M. Baugh, C.F. Randell, J. Appl. Electrochem. 17 (1987) 165.
[16] S. Atlung, T. Jacobsen, Electrochim. Acta 21 (1976) 575.
[17] S.R. Narayanan, D.H. Shen, S. Surampudi, A.I. Attia, G. Halpent, J. Electrochem. Soc. 140 (1993) 1854.
[18] M.G.S.R. Thomas, P.G. Bruce, J.B. Goodeough, J. Electrochem. Soc. 132 (1985) 1521.
[19] R. De Levie, Electrochim. Acta 8 (1963) 751.
[20] H. Von Helmhoz, Ann. Phys. 29 (1879) 337.
[21] G. Gouy, J. Phys. 9 (1910) 457.
[22] D.L. Chapman, Philos. Mag. 25 (1913) 475.
[23] O. Stern, Z. Elektochem. 30 (1924) 508.